Building an Alpha Spectrometer for the CUORE Collaboration

A Senior Project

By

David J. Miller

Advisor: Professor Thomas Gutierrez

Department of Physics
California Polytechnic State University San Luis Obispo

December 10, 2012

Approval Page

Title: Building an Alpha Spectrometer for the CUORE Collaboration

Author: David J. Miller

Date Submitted: December 8, 2012

Senior Project Advisor: Professor Thomas Gutierrez

_____

Signature

_____

Date

Contents

Abstract

This paper will give the reader a brief introduction to the Standard Model, Neutrinoless Double Beta Decay ($0\nu\beta\beta$), and the CUORE experiment under construction at Gran Sasso National Lab in Assergi, Italy. The remainder of the paper will describe the process of creating a working alpha spectrometry system using silicon detectors and NIM and CAMAC electronics. Extensive details of the troubleshooting and calibration period are presented as a way for the reader to better understand the concepts involved in alpha spectroscopy and to not repeat mistakes made in this development process.

"No amount of experimentation can ever prove me right; a single experiment can prove me wrong."–Albert Einstein [1]

1 Introduction

The Standard Model is a mathematical formulation that describes subatomic interactions. First formulated in the mid-twentieth century as a synthesis of many individual theories, the Standard Model accurately predicted half-a-century of discoveries in particle physics. First, the charm quark was observed in 1974 with the tau lepton and bottom quark being observed shortly thereafter. The W and Z bosons were seen in 1983 as predicted by the Standard Model. The top quark and tau neutrino were discovered at the end of the 20^{th} century and new results point to the existence of the last undiscovered[1] particle predicted by the Standard Model, the Higgs boson [2, 3]. The Standard Model is remarkable in that all, with the possible exception of the Higgs, of its predicted particles have been found. Although experimental results have been extremely consistent with the predictions made by the Standard Model, several unexpected results have been contradictory. One of these is the discovery that neutrinos oscillate between the three flavors of neutrinos: electron, muon, and tau. This discovery indicated that neutrinos have mass, opening the theoretical possibility that they may be Majorana fermions, which are a class of electrically neutral particles that are their own antiparticles. As of now, no fundamental Majorana fermions are known to exist. If the neutrino is in fact a Majorana particle, a rare type of decay known as neutrinoless double-beta decay ($0\nu\beta\beta$) is predicted to occur. In $0\nu\beta\beta$, the Majorana neutrino appears only in the virtual state leaving only two emitted electrons and the daughter particle in the final state. Several experiments around the world are searching for $0\nu\beta\beta$. The focus of this paper, CUORE (The Cryogenic Underground Observatory for Rare Events), is one such experiment. If CUORE is successful in finding $0\nu\beta\beta$, it would help to bring new discoveries related to neutrinos into the framework of the Standard Model.

This paper will attempt to give a cursory introduction to CUORE and the Standard Model; however, the crux of this paper will be on a small project that was worked on as part of the larger CUORE experiment. CUORE relies on maintaining an extremely low background to make it possible to distinguish the ultra-rare $0\nu\beta\beta$. As such, even trace amounts of radioactive contamination are a cause of major concern for the experiment. Degraded alphas occur in the region in which $0\nu\beta\beta$ is predicted to occur; thus, the ability to measure the alpha spectrum of various materials is vital to the experiment. Several proprietary commercial systems are currently in use by CUORE but the opportunity arose to attempt to refurbish an old and unused vacuum chamber and create a low cost, open-source alpha spectrometer using a silicon semiconductor detector as well as NIM and CAMAC modules.

2 Background

Before delving into the details of the alpha spectroscopy system, a brief introduction to the Standard Model, CUORE, and semiconductor detectors will be presented.

[1] At time of writing, the CMS and ATLAS collaborations had just announced the discovery of a Higgs-like particle. It is likely that this result will be confirmed in the near future.

2.1 Standard Model

Newton's laws explain the interactions in the world of classical physics, low velocities and intermediate masses, remarkably well. The natural question arises whether there is a simple set of laws that governs the dynamics and interactions of particles in the atomic and subatomic regime. Over the course of the 20^{th} century, a variety of experiments led to the discovery of a host of fundamental particles; composite particles made up of the fundamental particles; and the four types of interactions between them: gravitation, electromagnetic, strong nuclear, and weak nuclear. On the mass scales of these particles, the force of gravitation is roughly 40 orders of magnitude weaker than the other three forces and does not contribute to subatomic interactions in any meaningful way[2]. The Standard Model is a mathematical union of the three subatomic forces and the known subatomic particles that predicts the dynamics of the subatomic world.

Name	Symbol	Generation	Mass	Charge (e)	Spin	Antiparticle
Up	u	1	1.5-3.3 MeV/c^2	2/3	1/2	$\bar{u}$
Down	d	1	3.4-6.0 MeV/c^2	-1/3	1/2	$\bar{d}$
Charm	c	2	1.16-1.34 GeV/c^2	2/3	1/2	$\bar{c}$
Strange	s	2	70-130 MeV/c^2	-1/3	1/2	$\bar{s}$
Top	t	3	169.1-173.3 GeV/c^2	2/3	1/2	$\bar{t}$
Bottom	b	3	4.130-4.370 GeV/c^2	-1/3	1/2	$\bar{b}$

Table 1: The quarks of the Standard Model with corresponding mass, electrical charge, spin, and the symbols for the associated antiparticles [4].

Name	Symbol	Generation	Mass	Charge (e)	Spin	Antiparticle
Electron	e^-	1	0.511 eV/c^2	-1	1/2	e^+
Electron Neutrino	ν_e	1	<2.2 eV/c^2	0	1/2	$\bar{\nu_e}$
Muon	μ^-	2	105.7MeV/c^2	-1	1/2	μ^+
Muon Neutrino	ν_μ	2	<0.17 MeV/c^2	0	1/2	$\bar{\nu_\mu}$
Tau	τ^-	3	1.777 GeV/c^2	-1	1/2	τ^+
Tau Neutrino	ν_τ	3	<15.5 MeV/c^2	0	1/2	$\bar{\nu_\tau}$

Table 2: The leptons of the Standard Model with corresponding mass, electrical charge, spin, and the symbols for the associated antiparticles [4].

Name	Symbol	Mass	Charge (e)	Spin	Antiparticle
Photon	γ	0	0	1	γ
Gluon	g	0	0	1	g
Z Boson	Z	91.2 GeV/c^2	0	1	Z
W Boson	W^-	80.4 GeV/c^2	-1	1	W^+
Higgs Boson	H^0	125.3 GeV/c^2	0	0	H^0

Table 3: The bosons of the Standard Model with corresponding mass, electrical charge, spin, and the symbols for the associated antiparticles [4].

[2]Incorporating gravitation into the Standard Model in a universally consistent way, a so called 'Theory of Everything' is an area of active research in the particle physics community.

The Standard Model posits that there are two types of elementary particles, fermions and bosons. Fermions are classified further into the categories of quarks and leptons, each of which has three generations of particles. The particles of the Standard Model are listed in Tables 1, 2, and 3. Every particle has an associated antiparticle, a particle with internal quantum numbers of an opposite sign. Examples include electric charge and lepton number.

The class of particles known as bosons are characterized by integer spins ($\pm$ 1, $\pm$ 2, etc...) and their lack of obedience to the Pauli-exclusion principle, which allows multiple bosons to occupy the same quantum state. There are two types of elementary bosons, gauge bosons, which serve to carry interactions between particles, and the Higgs boson.

The Standard Model describes particle interactions as the exchange of gauge bosons; the electromagnetic force by the exchange of photons, the strong nuclear force by gluons, and the weak nuclear by the W and Z bosons [5]. Each of these gauge bosons carries with it a momentum and energy which are transferred from one particle to another giving the illusion of an invisible force acting. Gauge bosons couple and interact only with particles with specific types of internal quantum numbers. For example, the electromagnetic interaction occurs only between particles with electric charge and the strong interaction occurs between quarks of certain color quantum numbers. The strong interaction binds quarks together to form particles such as protons and neutrons. The combination of a quark and an antiquark forms a meson, such as a pion. The pion acts analogously to gluons within a nucleon; however, instead of binding quarks together to form a proton or neutron, it binds protons and neutrons together to form an atomic nucleus. This force is attractive and is what holds the nucleus together [2].

2.2 Radioactive Decay

Nuclear binding energy is the energy to fully disassemble a nucleus. This energy is a product of the competing attractive force of the nuclear interaction between nucleons and the repulsive force of electromagnetism between positively charged protons. An atomic nucleus will attempt to reach the most tightly bound state where the binding energy is at a maximum permitted under the Pauli-exclusion principle. A nucleus does this through a process known as radioactive decay. In radioactive decay, a nucleus will emit some number of particles and decay into a more tightly bound daughter nucleus. The Q-value of a decay is the rest mass of the parent nucleus minus the rest masses of the daughter nucleus and decay products. A decay can occur spontaneously when the Q-value is positive and conservation laws are satisfied. If this spontaneous decay occurs, the excess energy of the Q-value is distributed among the daughter nucleus and the decay products in the form of kinetic energy. In this paper, three types of radioactive decay are discussed: alpha decay, beta decay, and double beta decay.

In alpha decay, a helium nucleus, or alpha particle, quantum tunnels out of an atomic nucleus. The daughter particle thus loses two protons and two neutrons. This decay takes the following form,

$$ {}^{A}_{Z}N \longrightarrow {}^{A-4}_{Z-2}M + {}^{4}_{2}He^{2+} \tag{1} $$

with the alpha carrying off the majority of the energy from the Q-value, discussed in Section 3.7. The principle alpha decays in the transmutation of ^{226}Ra to ^{206}Pb are listed in Table 4 below.

The second type of decay is beta minus decay where a proton is transmuted into a neutron and an $\bar{\nu_e}$ and an e^-, known as a beta particle, are emitted. This is written as,

$$ {}^{A}_{Z}N \longrightarrow {}^{A}_{Z+1}M + e^- + \bar{\nu_e}. \tag{2} $$

Isotope	Decay Energy (keV)	Half-life
^{226}Ra	4784	1602 yr
^{222}Rn	5490	3.8 days
^{218}Po	6003	3.1 min
^{214}Po	7687	164 μs
^{210}Po	5304	1384 days

Table 4: The ^{226}Ra alpha decay chain. Rare decays such as the second ^{226}Ra are excluded [6].

A third type of process is the extremely rare simultaneous transmutation of two neutrons into two protons, known as double beta decay. In equation form,

$$ {}^{A}_{Z}N \longrightarrow {}^{A}_{Z+2}M + 2e^{-} + 2\bar{\nu_e}\,. \tag{3} $$

All of the particles emitted in the above decays can be characterized by how they are absorbed in matter. Particles passing through a material will lose energy in a variety of ways until they either exit the material or are stopped. When a particle stops in a material, the total energy deposited is equal to the initial kinetic energy of the particle. The change in kinetic energy over a given distance, dE/dx, can be either derived or found experimentally for different material and particle combinations. Thus, by measuring the energy deposited by a stopped particle in matter, the initial kinetic energy of the incident particle can be found. Both CUORE and semiconductor detectors use this method with CUORE relating a temperature increase to the deposited energy and semiconductors relating excitation of electron-hole pairs to the initial energy. Alpha particles and beta particles lose energy primarily through electromagnetic interactions. Electromagnetic energy loss is proportional to the square of the particle charge [7].

Since an alpha particle has charge +2, an alpha particle will lose energy four times as fast as an electron of the same velocity. A 4.8 MeV alpha will be completely stopped by 3.3 cm of air and significantly less distance in solids [7]. ORTEC cites a stopping distance of 30 μm for natural alpha particles in silicon and designs its detectors with silicon depths greater than this value as to stop all alphas completely. At the energies seen in $2\nu\beta\beta$ and $0\nu\beta\beta$, betas have a range of about 405 cm in air, 4.1 mm in water, and even less when passing through a solid [7].

2.3 Fermions and Neutrinoless Double Beta Decay

Fermions have several defining characteristics: all fermions have half-integer spin and by the spin statistics theorem, obey the Pauli-exclusion principle. The Pauli-exclusion principle states that identical fermions cannot occupy the same quantum state. Fermions can either be the elementary particles listed in Tables 1 and 2 or composite particles made up of these elementary particles, such as protons (uud) and neutrons (dud). Although quarks and leptons are both fermions, they differ in the fact that leptons are not subject to the strong nuclear force. As they are not directly related to CUORE, the details of quarks will be omitted for brevity's sake.

Leptons are divided into two different types with three generations (flavors) each and corresponding antiparticles. Each generation of lepton has its own associated quantum number (electron lepton number, L_e, for the e^- and $\bar{\nu_e}$; muon lepton number, L_μ, for the μ^- and ν_μ; and tau lepton number, L_τ, for the τ^- and ν_τ). A total lepton number, L, is also included. Lepton number is defined as the number of leptons minus the number of antileptons, $L = n_l - n_{\bar{l}}$. For example, a single electron or electron neutrino has $L = L_e = +1$ and a single antielectron

(positron) or electron antineutrino has $L = L_e = -1$. The Standard Model in its current form requires that lepton number, both total and generational, be conserved. An example of lepton number conservation can be seen in $2\nu\beta\beta$,

$$\begin{aligned} &{}^{A}_{Z}N \longrightarrow {}^{A}_{Z+2}M + 2e^- + 2\bar{\nu_e} \\ &\mathrm{N} \longrightarrow \mathrm{N} + 2 - 2 \text{ with } \Delta L = 0 \cdot \end{aligned} \tag{4}$$

The experimental result that neutrinos oscillate between three neutrino flavors showed a violation of generational lepton number while preserving total lepton number. These flavor oscillations cannot occur in a massless neutrino implying that neutrinos must be massive particles [8]. Massive neutrinos are in violation of the Standard Model and require that some modification be made to the Standard Model in order to include them. There are multiple ways to do this but an elegant and experimentally testable solution is to make the neutrino a Majorana particle, defined as a particle that is its own antiparticle. If this is the case, lepton number for the neutrino and antineutrino would not be $+1$ and -1 respectively but instead, there would be a single neutrino particle with two lepton number states. This would allow a massive neutrino to be compatible with the Standard Model [8]. As a consequence, some lepton violating processes would be expected to occur, one of which is $0\nu\beta\beta$. This decay, like $2\nu\beta\beta$, is the simultaneous decay of two neutrons into two protons. Instead of decaying into two neutrinos and two electrons in the final state however, $0\nu\beta\beta$ sees the Majorana neutrino appear only in the virtual state. This has the effect of leaving only two electrons and the daughter particle in the final state. Due to conservation of momentum and energy, the electrons are emitted with a precise energy equal to the Q-value minus the rest-mass of the two electrons and the kinetic energy of the recoiling daughter. Lepton number is not conserved in $0\nu\beta\beta$ as seen in the following decay equation,

$$\begin{aligned} &{}^{A}_{Z}N \longrightarrow {}^{A}_{Z+2}M + 2e^- \\ &\mathrm{N} \longrightarrow \mathrm{N} + 2 \text{ with } \Delta L = 2 \cdot \end{aligned} \tag{5}$$

Finding $0\nu\beta\beta$ would unequivocally violate lepton number conservation and show that massive particles may be Majorana particles. As $0\nu\beta\beta$ has been experimentally shown to be an extremely rare process if it exists, experiments must be designed in a way to detect such such rare decays [9].

2.4 CUORE

CUORE, a scaled up version of a previous experiment, Cuoricino, is among a handful of experiments searching for $0\nu\beta\beta$ but one of only several to use the bolometric technique. As explained above, when particles travel through matter, they transfer kinetic energy to the material they are passing through. A bolometric detector relates a temperature increase of the detection medium to the kinetic energy deposited by a particle. If the particle is stopped completely, a medium's increase in temperature can be related to the initial kinetic energy of the particle.

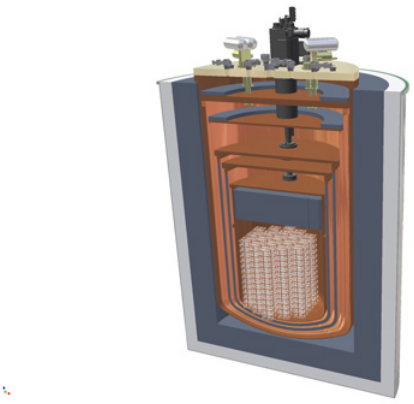

Figure 1: A CAD mockup of the CUORE cryostat and detector. CUORE consists of a large cryostat with several layers of lead and copper shielding. Housed inside is the detector array [10].

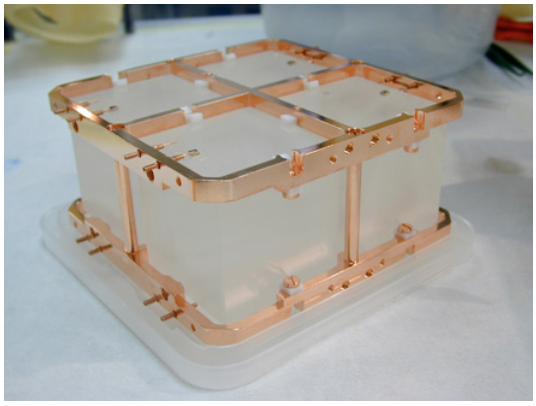

Figure 2: A Single Level of the Cuoricino tower. The tower levels in CUORE will appear very similar to the Cuorcino levels [10].

There are two key components to the CUORE detector: TeO_2 crystals and neutron transmutation doped germanium thermistors (NTDs). CUORE uses 988 TeO_2 crystals as a detection medium held in a 19 tower array, shown in Figure 1. Each individual tower consists of 13 levels of 4 crystals each with each level appearing similar to the Cuoricino level seen in Figure 2. This gives a total of 52 crystals per tower.^{130}Te, with a $0\nu\beta\beta$ Q-value of 2527 keV, is one of few isotopes which undergoes $2\nu\beta\beta$ (and thus are candidates for $0\nu\beta\beta$) and is unique among other $0\nu\beta\beta$ candidates in that it has a relatively large natural abundance of 33.8% [11]. The next highest natural abundance is in ^{110}Pd at 11.8% [9]. This allows CUORE to employ a large mass of TeO_2, 741 kg total, with an active mass of 206 kg ^{130}Te, without the expensive process of enriching[3] the crystals to contain a higher percentage of ^{130}Te.

Each individual CUORE crystal has two items precision glued to it: an NTD and a heating chip. An NTD is a semiconductor that acts as an extremely sensitive thermistor. This sensitivity

[3] One possible upgrade path for CUORE is to enrich the TeO_2 crystals to much higher percentages of ^{130}Te which would increase the number of $2\nu\beta\beta$ decays and of $0\nu\beta\beta$ decays if they do in fact occur [8].

is achieved by adding impurities to the germanium changing its properties. This is known as doping the germanium. The sample that is to be doped is exposed to a neutron source for some period of time. Neutrons are captured by nuclei in the sample at a rate dependent on the neutron cross section of the material and the nuclei enter excited states. These states then decay into a more stable configuration. Three natural germanium isotopes ($^{70}_{32}$Ge, $^{74}_{32}$Ge, and $^{76}_{32}$Ge) undergo this process in a germanium NTD. The reactions are given below,

$$^{70}_{32}\mathrm{Ge} + \mathrm{n} \longrightarrow \gamma + {}^{71}_{32}\mathrm{Ge} \tag{6}$$
$$^{71}_{32}\mathrm{Ge} + \mathrm{e}^- \xrightarrow{\tau_{1/2}=11.4 \text{ days}} \nu_e + {}^{71}_{31}\mathrm{Ga}$$

$$^{74}_{32}\mathrm{Ge} + \mathrm{n} \longrightarrow \gamma + {}^{75}_{32}\mathrm{Ge} \tag{7}$$
$$^{75}_{32}\mathrm{Ge} \xrightarrow{\tau_{1/2}=83 \text{ min}} \mathrm{e}^- + \overline{\nu_e} + {}^{75}_{33}\mathrm{As}$$

$$^{76}_{32}\mathrm{Ge} + n \longrightarrow \gamma + {}^{77}_{32}\mathrm{Ge} \tag{8}$$
$$^{77}_{32}\mathrm{Ge} \xrightarrow{\tau_{1/2}=11.3 \text{ hrs}} \mathrm{e}^- + \overline{\nu_e} + {}^{77}_{33}\mathrm{As}$$
$$^{77}_{33}\mathrm{As} \xrightarrow{\tau_{1/2}=38.8 \text{ hrs}} \mathrm{e}^- + \overline{\nu_e} + {}^{77}_{34}\mathrm{Se}\,.$$

Natural germanium has the dopants $^{77}_{34}$Se, $^{75}_{33}$As, and $^{71}_{31}$Ga added to it through this method of doping. Neutron transmutation doping is favorable as it allows for very uniform doping of germanium in amounts proportional to the neutron flux. The half-lives of the decays are short enough that all the of the neutron activated isotopes decay away so as to not contribute to the CUORE background [12]. By gluing an NTD to a TeO_2 crystal, it becomes possible to detect $0\nu\beta\beta$. If $0\nu\beta\beta$ occurs in a ^{130}Te atom, the two emitted electrons plus the parent recoil will deposit their energy into the crystal raising its temperature by a small amount. The NTD is in thermal contact with the crystal so it will experience the same temperature increase as the crystal. This appears as a voltage pulse since the temperature of the NTD rises and is then removed by the cryostat. Thoriated wires are used to calibrate the voltage pulse to energy deposited. Since thorium has a well known gamma spectrum, the voltage pulse for each individual peak in the thorium spectrum can be directly related back to a deposited energy. This allows voltage pulses from other events to be matched to the initial energy deposited in the crystals. The crystals must be kept at an extremely low temperature, on the order of 10 mK, since heat capacity scales like T^3 according to the Debye law [13]. A low heat capacity leads to greater temperature increases with energy deposition events. This in turn leads to a larger change in the resistance of the NTDs and corresponding voltage spike. Larger voltage spikes rise higher above the electronic noise and thus offer a better resolution. If the temperature is too high, events on the order of 2527 keV would not raise the temperature of the crystal by an appreciable amount [13]. The heating chips are used to apply exact amounts of energy to the crystals to provide a means of calibrating the detector for temperature drifts[13]. If $0\nu\beta\beta$ occurs in ^{130}Te, the energy deposited by the electrons will be at about 2527 keV. In this way, the TeO_2 crystals act both as the source for the decay trying to be found and also as part the detector itself. Since the crystal array is housed in a large dilution refrigerator, the excess heat generated from the decay is quickly removed by the cryostat and the crystal returns to base temperature.

The current bolometric technique in use by CUORE has no particle identification so the electrons emitted during $0\nu\beta\beta$ cannot be discerned from other particles depositing 2527 keV

in the TeO_2 crystals. Since $0\nu\beta\beta$ has an extremely small decay rate, even an extremely small number of extraneous counts in the region of interest will make it impossible to distinguish the $0\nu\beta\beta$ signature from the background radiation.

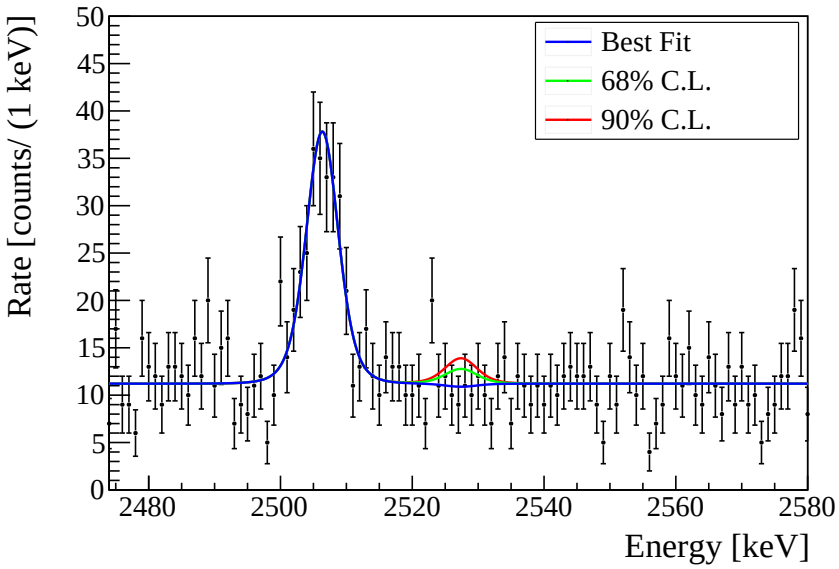

Figure 3: Cuoricino data in 2527 keV region over the course of its run time. A best fit is displayed in blue and what would be 68% and 90% confidence levels for a $0\nu\beta\beta$ signal are overlaid [14].

Figure 3 shows the data in the region of interest for $0\nu\beta\beta$ taken from the two runs of the Cuoricino experiment over the course of 5 years. The problem of background radiation is illustrated here. The blue line shows a fit applied to the histogram of counts/keV versus energy. The lines for confidence levels of 68% and 90% for $0\nu\beta\beta$ are overlaid at 2527 keV. The background level in the region, effectively the blue line in Figure 3, was too high to detect $0\nu\beta\beta$ if it occurs. Although the experiment did not detect the decay, it was able to set a limit on the half-life of the decay by establishing the background and relating it to the rate of decay that would have produced a visible signal. This analysis method set the limit on the half-life of $0\nu\beta\beta$ in ^{130}Te at $\tau^{0\nu}_{1/2} = 2.8 \times 10^{24}$ yr with a 90% confidence level.

CUORE hopes to achieve a significantly better limit on the half-life[4] of $0\nu\beta\beta$ in ^{130}Te on the order of $\tau^{0\nu}_{1/2} = 1.6 \times 10^{26}$ yr [15]. This value for $\tau^{0\nu}_{1/2}$ is derived from the theoretical half-life limit given in [15],

$$\tau^{0\nu}_{1/2} \propto \sqrt{\frac{M \cdot t}{b \cdot \delta E}} \tag{9}$$

where M is the total active mass; t is the active run time of the experiment in years; b is the background rate in counts/(keV·kg·yr); and δE is the energy resolution of the experiment. Since M and t are variables related to experimental design and are limited by cost and feasibility and δE is an intrinsic property of the TeO_2 crystals, lowering the background is the most immediate way to increase the sensitivity of the detector. Cuoricino achieved a background count rate in

[4] Assuming b=0.01 counts/(keV·kg·yr), δE=5 keV, a 1 sigma confidence level, and a run time of five years.

the $0\nu\beta\beta$ region of interest of b=0.18 counts/(keV·kg·yr). The goal of CUORE is to achieve a rate of b=0.01 counts/(keV·kg·yr) but a rate of b=0.001 counts/(keV·kg·yr) is thought to be possible [16]. Simulations have shown that roughly 70% of the CUORE background in the 2527 region is due to degraded alpha particles which makes alpha background reduction an important area of study [16, 17].

As mentioned in Section 2.2, alpha particles have a high dE/dx through solids. Alpha decays occurring more than several microns deep in a solid will be completely absorbed. However, an alpha decay near the surface of a solid will emit an alpha particle with a characteristic decay energy but that alpha will lose some amount of energy in the solid before exiting and entering free space. These energy-depleted particles are known as degraded alphas. Alpha-emitting isotopic contamination near the surface of any of the detector components (Copper frames, copper enclosure, TeO_2 crystals, etc...) all will produce degraded alphas and unlike natural alpha particles whose energies fall in the 3-8 MeV range, depleted alphas are emitted over a wide energy spectrum and can have energy in the 2527 keV range. Alpha particles with this energy contribute to the background covering the $0\nu\beta\beta$ signal. Much ongoing research is occurring within the CUORE collaboration in regards to preventing or mitigating the problem of degraded alphas.

2.5 Silicon Charged Particle Detectors

The alpha spectrometry system detailed in the following section was based around an ORTEC A-series[5] This brief section will discuss the basic principles of a semiconductor detector, and in particular, silicon detectors. A more extensive discussion is presented in [18] and several books are written purely on the properties of silicon detectors [19]. Silicon charged particle detectors rely on the fact that energy deposited in a semiconductor excites electrons out of the valence band into the conduction band.

In a semiconductor, the energy difference between the two bands, called the bandgap, is very small, on the order of 5 eV, and very little excess energy is required to excite electrons into the conduction band. In the valence band, since the entire outer atomic shell is filled, the Pauli-exclusion principle disallows electrons from moving between atoms. Once in the conduction band however, electrons can move freely between atoms as there is an abundance of empty electron shells at the same energy level as the exited electron. When an electron is excited out of the valence band, it leaves behind a empty spot, known as a hole. Since this hole in the valence band is now unfilled, electrons are free to move into the unfilled spot. When an electron moves into the unfilled spot, it creates another hole which can be filled. In this way, the hole appears to move like a positively charged particle. After some amount of time, the electron will emit a photon and return to the ground state recombining with the hole.

An alpha particle, with energy on the order of 5000 keV, entering a semiconductor deposits all of its energy in the crystal lattice and creates an abundance of electron hole pairs. If an electric field is applied to the semiconductor, the electrons will flow towards the cathode and holes will flow towards the anode with a velocity defined as the drift velocity. A circuit may be made by creating a conductive path from the anode to the cathode, which allows electrons to flow out of the semiconductor. If the electric field is of sufficient strength, all electron-hole pairs will exit the semiconductor into the circuit. Current is defined as the change in current during

[5]The ORTEC U-series of detectors is now used in most alpha spectroscopy applications where an A-series was used previously. The A-series was used due to availability.

a time interval, I=$\frac{dq}{dt}$. Since charge is conserved, all initially liberated charge passes through the circuit. Energy is proportional to the initial amount of charge liberated and thus,

$$E \propto Q = \int_{t_i}^{t_f} I \, \mathrm{d}t. \tag{10}$$

Various electronic configurations can perform this integral to find the energy of the incident alpha. In the case of the alpha spectroscopy system described in this paper, an ORTEC charge sensitive preamplifier integrates this charge and outputs a voltage pulse with height proportional to the energy deposited. The preamplifier also is able to supply the bias voltage which generates the charge collecting electric field. This is a much simplified description of a semiconductor detector. In practice, a semiconductor must be doped in order to perform well as a radiation detector.

Many factors which are presented in [18] affect the performance of a silicon detector but the description given above will be sufficient for the scope of this paper. The main performance parameter used is the resolution of the detector. Resolution is the spread of energies measured around the central known energy peak. This value is typically measured in full-width half-maximum which is related to the standard deviation of a guassian by FWHM=$2\sqrt{2\ln 2}\cdot\sigma$ Many factors affect resolution of the detection system such as electronic noise, size of the detector, length of cable between detector and preamp, and even the geometry of the detector to source among other factors. Attempts were made to minimize these factors throughout the system.

At this point, this paper will transition into a detailed description of the spectrometer.

3 Assembly, Development, and Calibration of a Non-Commercial Alpha Spectrometer

CUORE relies on maintaining an ultra low background in the 2527 keV region where $0\nu\beta\beta$ is expected to occur. Therefore, it is extremely important to perform accurate measurements of the alpha spectrum of materials exposed to the CUORE detector. Alpha particles are particularly problematic as the degraded alphas are impossible to differentiate from a real $0\nu\beta\beta$ signal. Additionally, alpha spectrometers may be used for a variety of other measurements. One example of this is as a means of measuring a thin film's thickness. This is done by taking measurements of a radioactive source with the thin film in place and then removed. A shift in energy will occur due to alphas depositing energy in the material. This loss of energy can then be related to the thickness of the material.

ORTEC, Canberra, and other companies make expensive off the shelf systems for alpha spectroscopy, several of which are in use by CUORE. Counting times for alpha spectroscopy can be weeks to months so multiple spectrometers are useful. Instead of acquiring a new commercial system, the decision was made to try to refurbish an old vacuum chamber and then use NIM and CAMAC modules and open source software to create a custom spectrometer. Although cost was the motivation for opting for this custom method, it offers several advantages, the foremost being that it is easier to modify the spectrometer if the need arises. For example, BNC feedthroughs are installed on the custom chamber if the need arises for more data read-out from inside the chamber.

The following sections will first detail the operational setup in a manner such that a similar system could be built; then will go through the trial and error process of setting up the system;

and finally, examine some of the considerations that must be made with an alpha spectrometer, such as recoil contamination and geometric efficiency.

3.1 Chamber and Pump

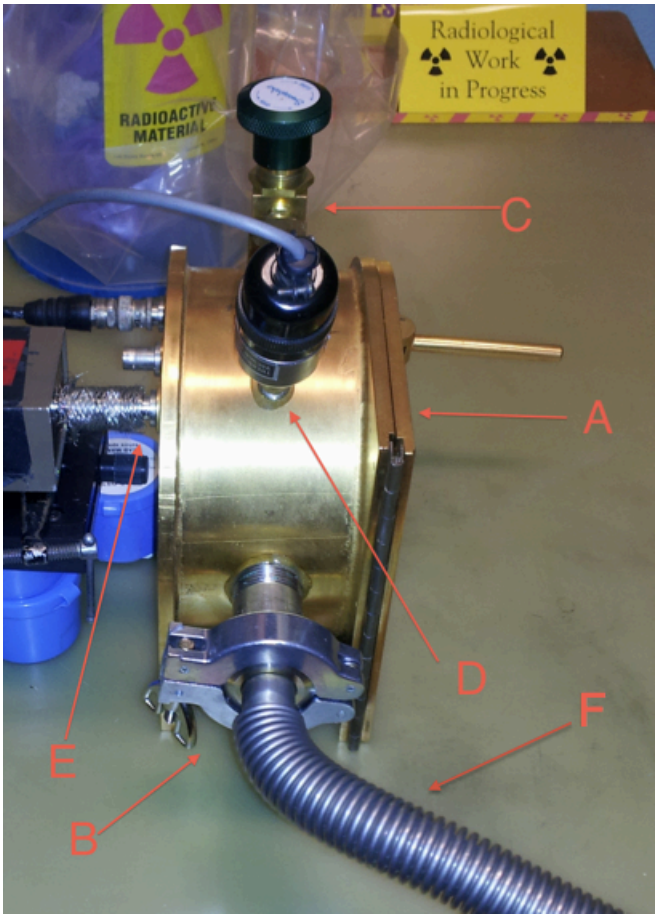

Figure 4: External view of the vacuum chamber used for the alpha spectrometer. Descriptions of the labeled components are presented below.

The core of the system is a refurbished vacuum chamber, Figure 4, made out of an unknown material with a hinged door [A]. The door closes onto an O-ring to establish a vacuum. A KF25 fitting [B] is welded to side of the chamber and a vent valve [C] and thermocouple vacuum gauge [D] are attached to the top of the chamber. There are three BNC feedthroughs on the backside of the chamber [E]. A metallic vacuum hose [F] is attached to the KF25 fitting on one end and a molecular sieve filter filled with zeolite[6] on the other end. This filter is directly connected to an Alcatel 2012A rotary vane vacuum pump. The purpose of the zeolite filter is to prevent oil from flowing out of the pump and into the chamber introducing contamination. With this pumping mechanism, a vacuum of 8 mTorr in the chamber can be achieved.

[6]Zeolite is a type of porous material that is very absorbent. It readily absorbs vapors and particles and is often used to prevent oil vapor from flowing into a vacuum chamber when the vacuum is released

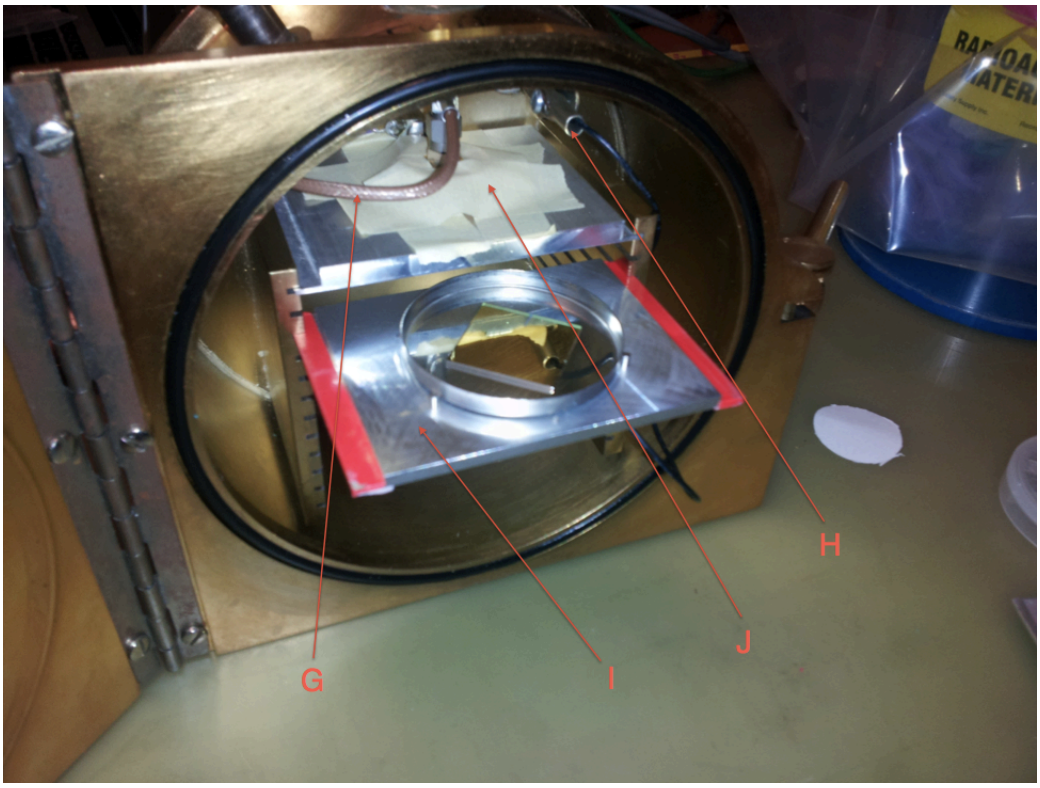

Figure 5: Internal view of the vacuum chamber. Descriptions of the labeled components follow.

A microdot wire [G] is spliced open on one end and soldered to the inside of one of the BNC feedthroughs. An alligator clip [H] is attached to the inside of another BNC feedthrough and the wire is taped to the bottom of the source plate [I]. This was done in order to establish a negative bias on the source plate to combat recoil contamination (see Section 3.7). Twelve evenly spaced slots were welded to the rear inside wall of the chamber. A plate in the top slot held the silicon detector [J] while the source plate in one of the lower slots held the various samples to be counted. Tape was used to stabilize the silicon detector.

3.2 Detector

The chamber can be outfitted with different size microdot connector equipped ORTEC A-Series detectors depending on the type of measurement. Detectors with active areas ranging from 150 mm^2 to 450 mm^2 were used while building and using the system. The spliced microdot wire is attached to the microdot jack on the back of the A-Series detector.

3.3 Data Acquisition

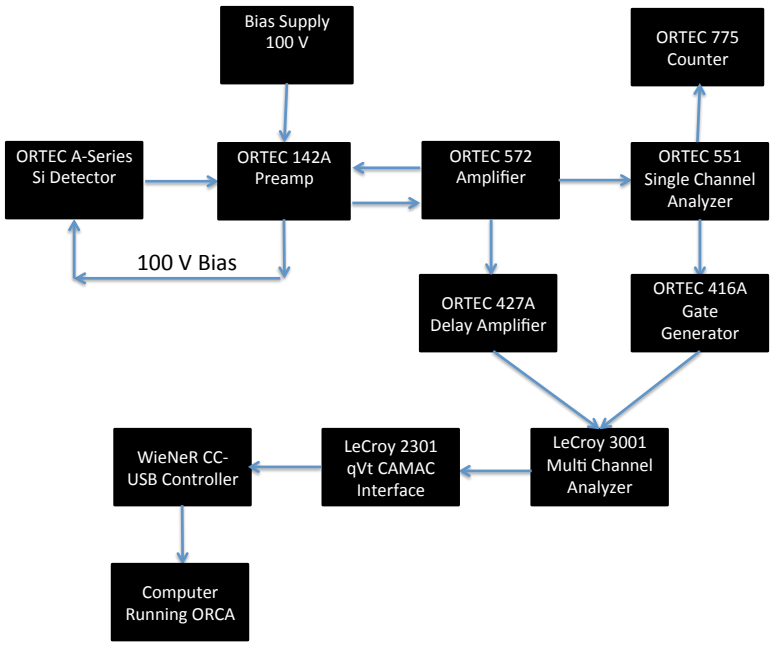

Figure 6: The electronics used in data acquisition. Each of these individual components will be described below.

Figure 6 diagrams the pulse processing and data acquisition process. Each component of the chain will be described below.

ORTEC 710

The ORTEC 710 Quad Bias Supply applies a bias voltage of between 1 and 1000 volts selectable on the front panel. Functionality for an automatic shutdown is incorporated in the event of vacuum loss but has not presently been implemented.

ORTEC 142A

The ORTEC 142A preamplifier is a type of amplifier known as a charge-sensitive preamplifier. As described in Section 2.5, incident radiation on the semiconductor excites an amount of charge proportional to the energy of the incident alpha particle. The charge is then collected by an external electric field creating a current. In a charge-sensitive preamplifier, the current charges a feedback capacitor in the preamplifier. Since all of the initial liberated charge is conserved, the charge on the feedback capacitor is equal to the charge liberated by the initial event. The preamplifier produces a voltage pulse proportional to the charge built up on the capacitor. If needed, the preamplifier can also generate a timing pulse. The preamplifier accepts a test pulse generated by a pulser for calibration purposes and also has an input for a bias voltage for the detector.

ORTEC 572

The ORTEC 572 Linear Amplifier accomplishes two tasks: first, it amplifies the voltage pulse to give the user control of the peak height. This is useful in setting what channel a certain energy corresponds to on an MCA. Secondly, the 572 shapes the voltage pulse to remove the long pulse tail generated by the preamplifier. Both of these tasks are accomplished while retaining linearity in the height of the voltage peak. Although less important in low count rate applications, removing the long tail of the voltage pulse is crucial in reducing pulse pileup. The shaping time and amplifier gain are both externally adjustable and are set depending on the application.

ORTEC 551

The ORTEC 551 Single Channel Analyzer generates a timing pulse when a signal pulse arrives desired amplitude. Front panel controls allow the user to set a voltage window, falling between 0 and 10 V, where this timing pulse is generated.

ORTEC 416

The ORTEC 416 Gate & Delay Generator accepts a triggering pulse and upon its arrival, generates a negative gate pulse with adjustable amplitude (2-10 V), width (ranging from 0.4 μs to 4 μs) and delay (ranging from 0 s to 11 μs). A gate pulse is used to set a time window for another module to be active. In this case, it sets the window where the MCA searches for a voltage peak.

ORTEC 427

The ORTEC 427 Delay Amplifier allows for a pulse to be delayed by up to 4.75 μs. Delays are needed since different modules offer different amounts of inherent delay and multiple inputs to some components must be arrive at precise timing. For example, the start of the gate pulse must arrive at the MCA just prior to the peak of the data pulse.

ORTEC 775

The ORTEC 775 Counter counts pulses that arrive with height over a set discriminator value.

LeCroy 3001

The LeCroy 3001 qVt acts similarly to any MCA. An event which occurs at a certain amplitude (charge, voltage, time, etc...) generates an entry in one of 1024 channels. Other events will generate entries in other channels related to the amplitude of the event. A histogram is then generated when number of events is plotted versus channel number. A well-functioning linear MCA maintains linearity across all channels so a linear calibration may be applied. The 3001 has three analysis modes: q mode, where the 3001 analyzes the area of a pulse; V mode, where it analyzes the height of a pulse; and t mode, where it analyzes the length of a pulse. As charge has already been integrated into a pulse with height proportional to the initial energy deposited by the incident alpha, the qVt was set to V mode. In V mode, the 3001 accepts voltage pulses between 1 mV and 1 V giving a resolution of about 1 mV/channel. Any pulses greater than 1 V are binned into channel 1024. The 3001 may be operated in several triggering modes ranging

from internal-triggering to external-triggering to external gated. For greater control over the the trigger, the external gate mode is used. In this mode, the 3001 searches for a voltage peak when triggered by a negative square gate pulse. The leading edge of the gate pulse should occur just before the voltage peak and end just after in order to not capture multiple voltage peaks.

LeCroy 2301

The LeCroy 2301 qVt to CAMAC interface reads data of off the 3001 and writes it into the CAMAC dataway which may then be transferred to a computer.

WieNeR CC-USB

The WieNeR CC-USB controller interfaces a computer to the CAMAC dataway allowing commands to be sent to components and data to be read from components.

ORCA

The data acquisition software ORCA was used to interface with the CAMAC electronics as well as to analyze data. ORCA is an open source program built for Mac OSX which is designed to control and read data from a host of scientific components with a computer interface.

3.4 Current Setup

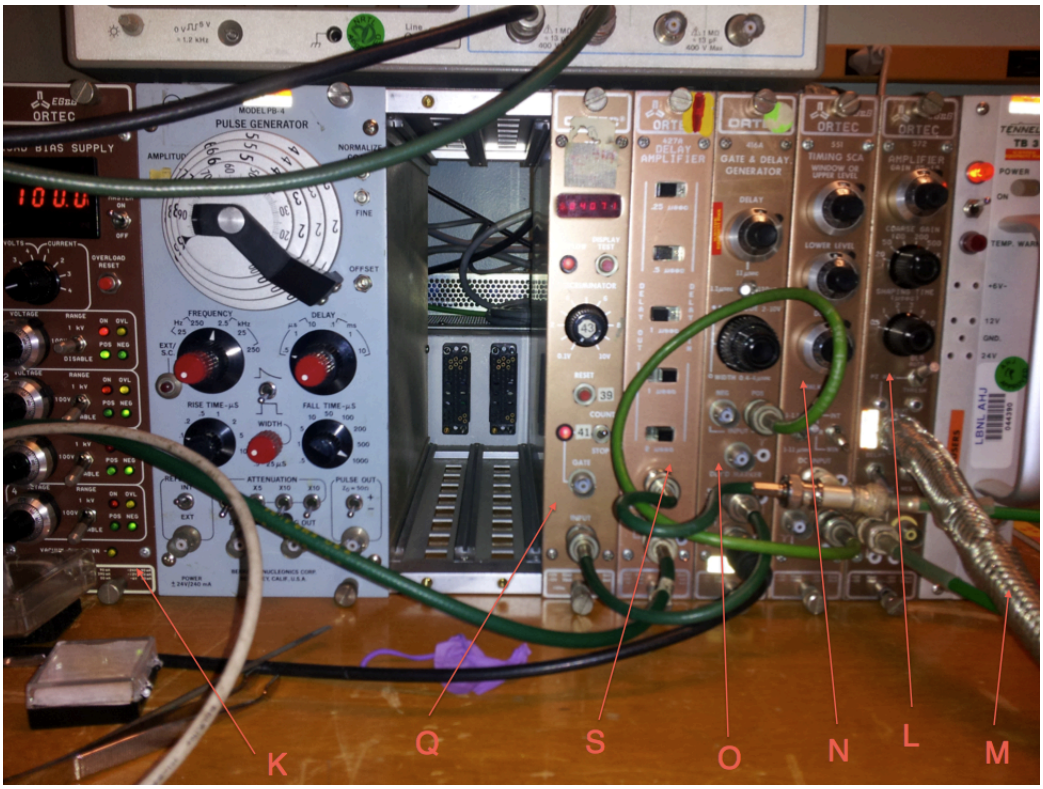

Figure 7: The NIM crate which held the DAQ electronics. A detailed description of the electronics follows.

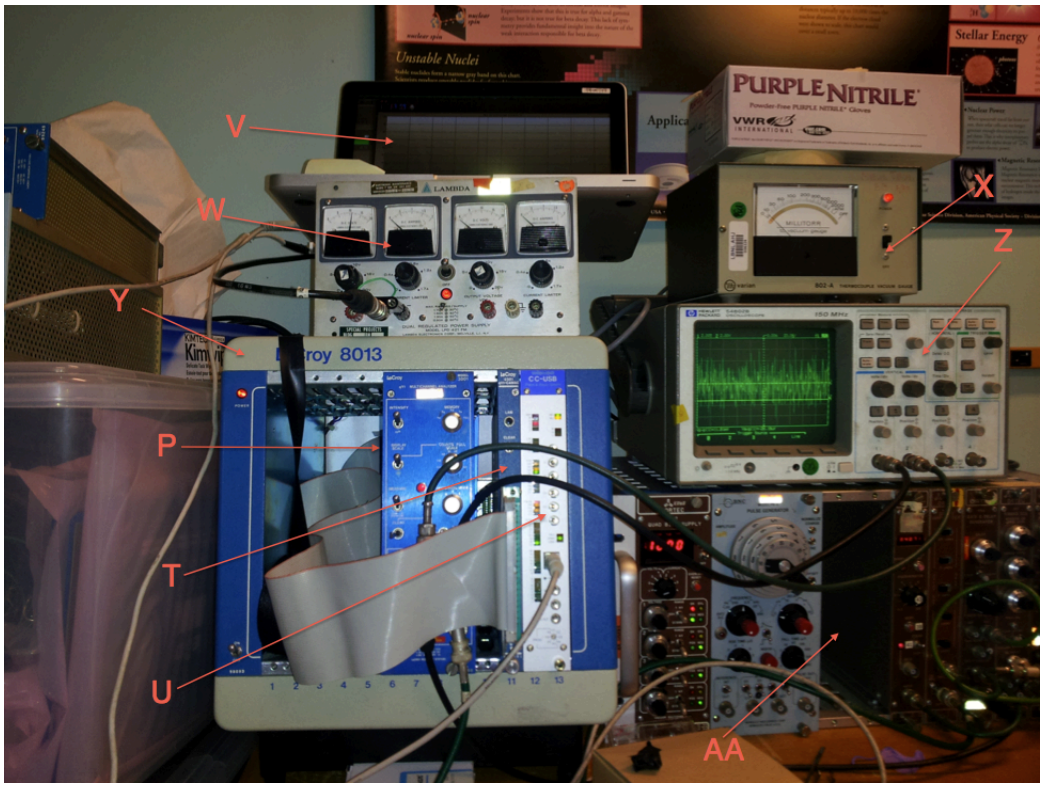

Figure 8: The CAMAC crate and other components in the system. The components labeled will be described below.

The detector BNC feedthrough from the vacuum chamber is connected to the 142A preamplifier [not pictured]. The preamplifier is connected to the BNC feedthrough with a BNC female-to-female connector in order to reduce the distance between the detector and preamplifier as to reduce electromagnetic noise introduced prior to amplification. The bias input on the 142A is connected to the 710 bias supply [K] by way of an SHV cable.

The voltage pulse from the 142A is then fed into a 572 linear amplifier [L] using an electromagnetically shielded BNC cable [M]. As this pulse is still to be amplified, any electromagnetic noise will be amplified as well greatly increasing the overall noise in the pulse and lowering the resolution attained. The course gain is set at an amplification factor of $\times 50$ and the fine gain is set at an amplification factor of $\times 0.7$, giving a total gain of $\times 35$, based off the system calibration (see Section 3.5). The shaping time is set a 0.5 μs as per ORTEC's recommendation for A-Series silicon detectors.

The amplified and shaped pulse from the unipolar output on the 572 is split into two channels. The first channel is the gate generation channel where the pulse is first fed into the input of the 551 SCA [N]. The 551 is set to generate a timing pulse for signal pulses with an amplitude between 50 mV and 1 V. Initial versions of the system forwent the 551 and pulse pileup was seen due to noise peaks below 50 mV. The window from 50 mV and 1 V corresponds to calibrated energies from 1500 to 9000 keV, which includes the energies of almost all natural alpha particles. The timing pulse generated by the 551 triggers the 416A gate generator [O] which in turn generates a gate pulse. This gate pulse is then fed into the gate input on the 3001 [P]. The gate

generator also outputs a positive square pulse which feeds the 775 counter [Q]. The 775 counts the registered signal pulses in order to determine whether the 3001 [R] is registering all pulses. For very radioactive sources, pulse pileup became an issue and the raw counts measured by the 775 did not match the number of counts registered by the 3001. For low counting applications, the numbers were seen to line up perfectly. The second channel is the data channel. The data signal is fed from the 572 into the 427A [S] where the pulse is delayed. The pulse is then fed into the V input on the qVt. The data pulse and gate pulse were timed to arrive at the same time. When looked at on an oscilloscope [Z], the leading edge of the gate pulse arrived during the rising edge of the signal pulse and the trailing edge arrived on the falling edge. The NIM electronics above were held in a generic NIM crate [AA].

The 3001 is set to V mode and the full 1024 channels are used to collect data. On the rear of the 3001, a 44-contact connector is connected to the front panel of the 2301 [T]. The WieNeR CC-USB Controller [U] is then connected to an Apple Macbook Pro running OSX Version 10.7.5 [V] and the latest build of ORCA with a custom driver written for the 2301. The 3001, CC-USB, and 2301 were held in and powered by a LeCroy 8013 crate [Y]. The 3001 is powered by the 8013 using a NIM to CAMAC adapter. A Varian vacuum gauge [X] displays the vacuum in the chamber and a power supply [W] applies a negative voltage to the source plate.

3.5 Development

The alpha spectroscopy system described above was developed through extensive research and trial, and error. The project began as a continuation of work done by Sam Meijer (Cal Poly) who worked to refurbish a vacuum chamber for the purpose of creating a functioning alpha spectrometer. The initial system consisted of a sorption pump[7] connected to the vacuum chamber and a 450 mm^2 ORTEC A-Series silicon detector. The detector was connected to the 142A preamp and then into the 3001, which was set to display its memory onto an oscilloscope in XY mode. Pulses were visible on a second oscilloscope after preamplification but no meaningful data could acquired with the 3001. A driver[8] for ORCA had previously been written for the 2301 which had been shown to compile and run but had not been used for data acquisition purposes.

ORTEC's published guide [20] for an setting up an alpha spectroscopy system using their specific data acquisition software and specific components was used as a starting point for further development. The 572 Amplifier was immediately added to the system which shaped the pulse and gave control over pulse heights. The gain on the 572 was eventually adjusted during calibration to place voltages corresponding to incident alpha energies of roughly 5000 keV near the central channel of the MCA. This allowed the MCA to detect alpha energies of 0 to around 9000 keV, which encapsulates almost all known natural alpha energies. Several small modifications were made to the settings on the 3001 which allowed it to function with ORCA. Initial spectra taken from the detector showed an exceptionally high count rate in the noisy 5 mV to 50 mV region and many apparently random counts at higher voltage regions. The internal threshold on the 3001 was used to discriminate against the low voltage regions and was successful but was not easily adjustable. This led to the inclusion of the 551 and 416 modules. A ^{226}Ra sealed source with a claimed source activity of 2778 Bq was also acquired to test and calibrate the system. With the source in the chamber, a massive increase in count rate was seen,

[7] A sorption pump is a vacuum pump which condenses air through cooling establishing a vacuum.
[8] The custom driver for the 2301 was written by by Sam Meijer in association with Jason Detwiler.

as would be expected with a radioactive source. No clear peaks were visible however.

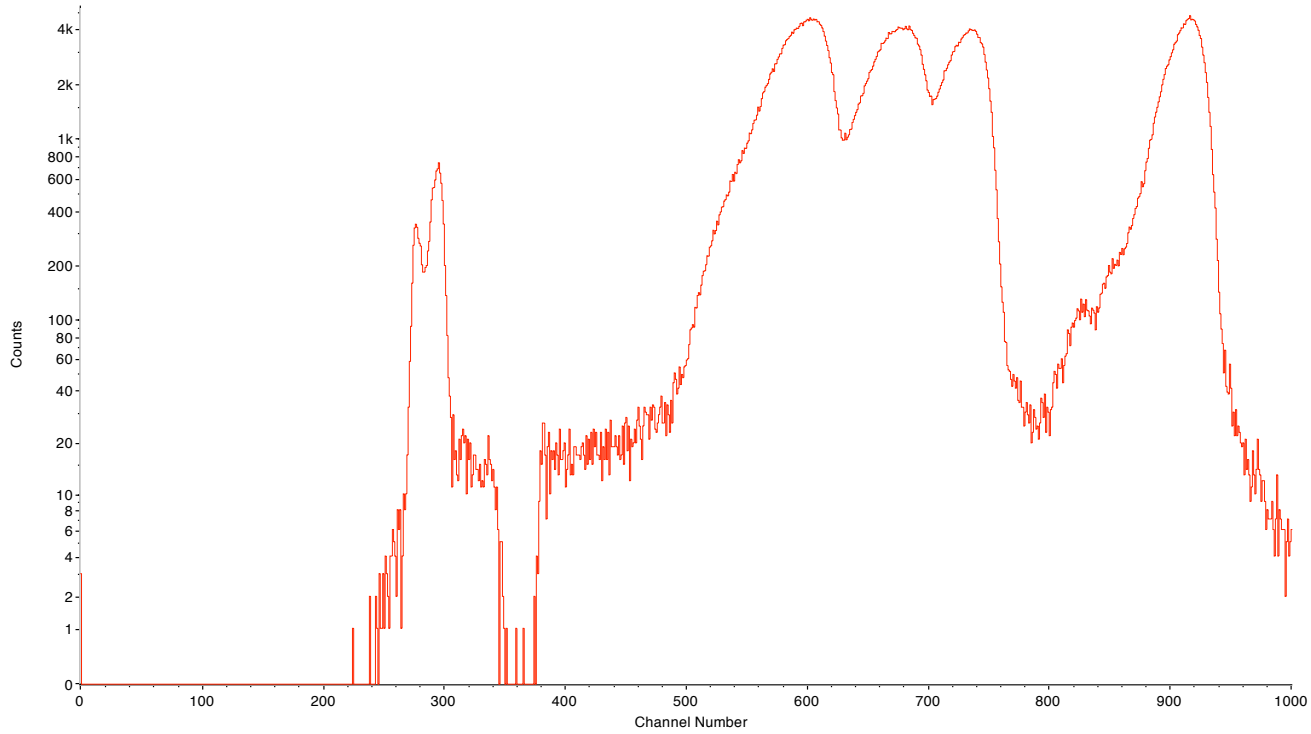

Figure 9: A spectrum taken of the ^{226}Ra source with vacuum of several Torr.

An unlabeled bias supply was being used at the recommended 75 V for an ORTEC A-Series detector. The unlabeled supply was replaced by the 710 and the bias was Increased to 300 V. At this voltage, peaks were clearly visible, seen in Figure 9. Up until this point, vacuum in the chamber was not being measured. ORTEC's vacuum pump purpose built for alpha spectroscopy is rated to achieve vacuum of 1 mTorr so this value was seen as a target pressure. The sorption pump being used at the time achieved an unknown vacuum so a thermocouple vacuum gauge was added to the system. This gauge showed that upon the initial cooldown of the sorption pump, pressures of several Torr could be achieved. Subsequent cooldowns were above the region measured by the gauge. Alphas are known to have high energy loss per unit length in air so high operating pressures would explain the broad spectrum in Figure 9 [18]. To test this theory, the sorption pump was replaced with an Alcatel 2012A rotary vane pump, rated to 8 mTorr. After several minutes of pumping, the vacuum gauge showed that the chamber was indeed at 8 mTorr and a 1200 s spectrum was taken of the ^{226}Ra source. Lowering the pressure greatly increased the resolution and made the ^{226}Ra peaks clearly visible. At this point, a calibration was done using the locations of the peaks for ^{226}Ra and the known energies of the alpha decays in the ^{226}Ra decay chain listed in Table 4.

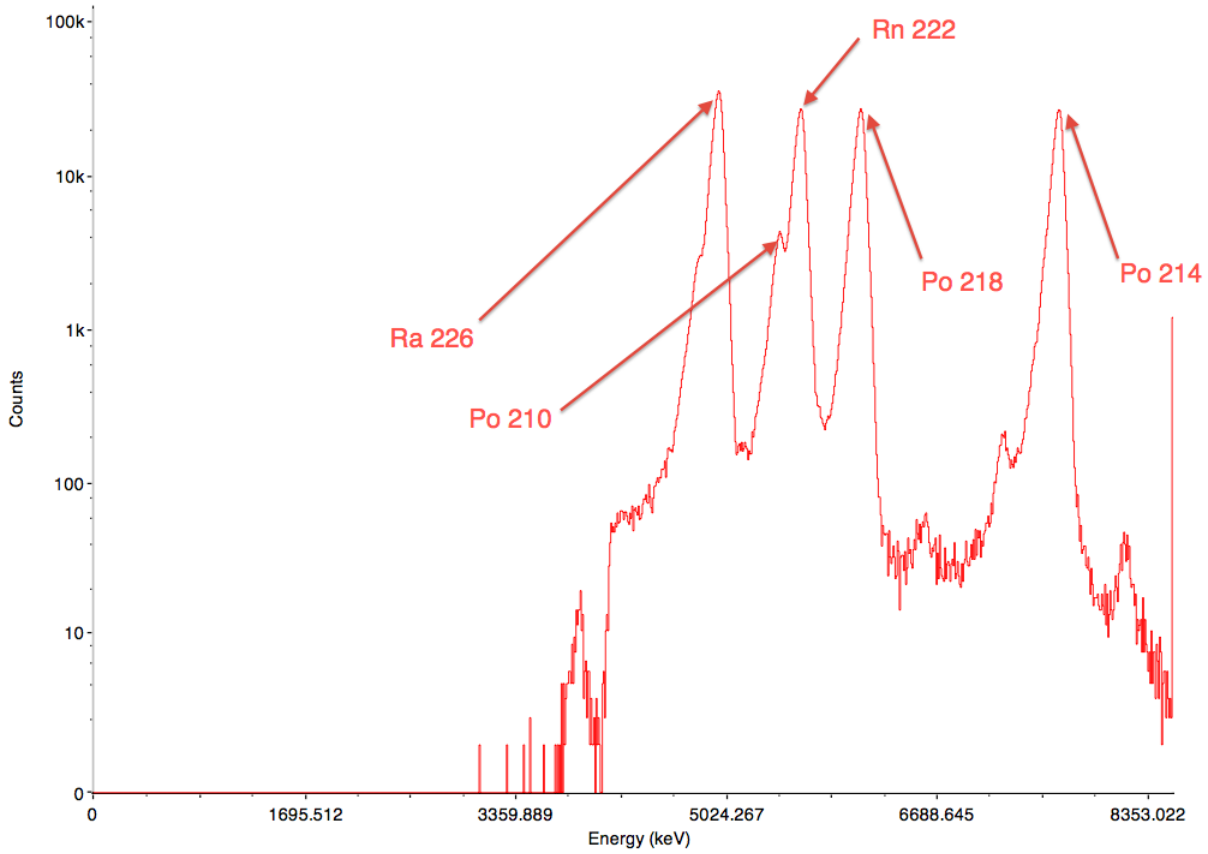

Figure 10: A spectrum taken of the ^{226}Ra source with background at 8 mTorr. A linear energy calibration has been applied and the peaks in the ^{226}Ra decay chain have been labeled.

Figure 10 shows the calibrated spectrum for the radium source. The resolution is increased significantly over Figure 9.

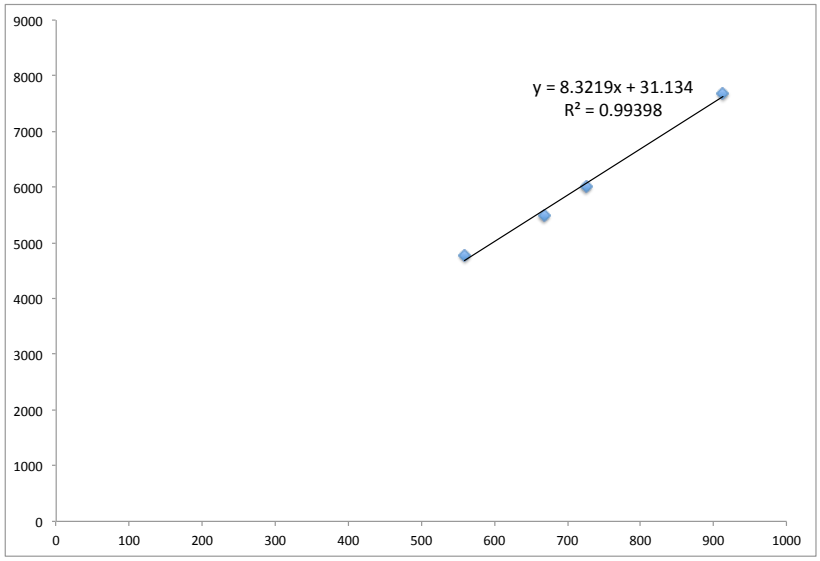

Figure 11: Linear fit of channel number vs. energy for ^{226}Ra calibration spectrum.

By plotting the energy versus the channel number and applying a linear fit, Figure 11, it was clear that the spectrometer had a linear response and that the calibration would hold across the entire energy spectrum. FWHM was found to be about 88 keV for the peaks in the ^{226}Ra decay chain.

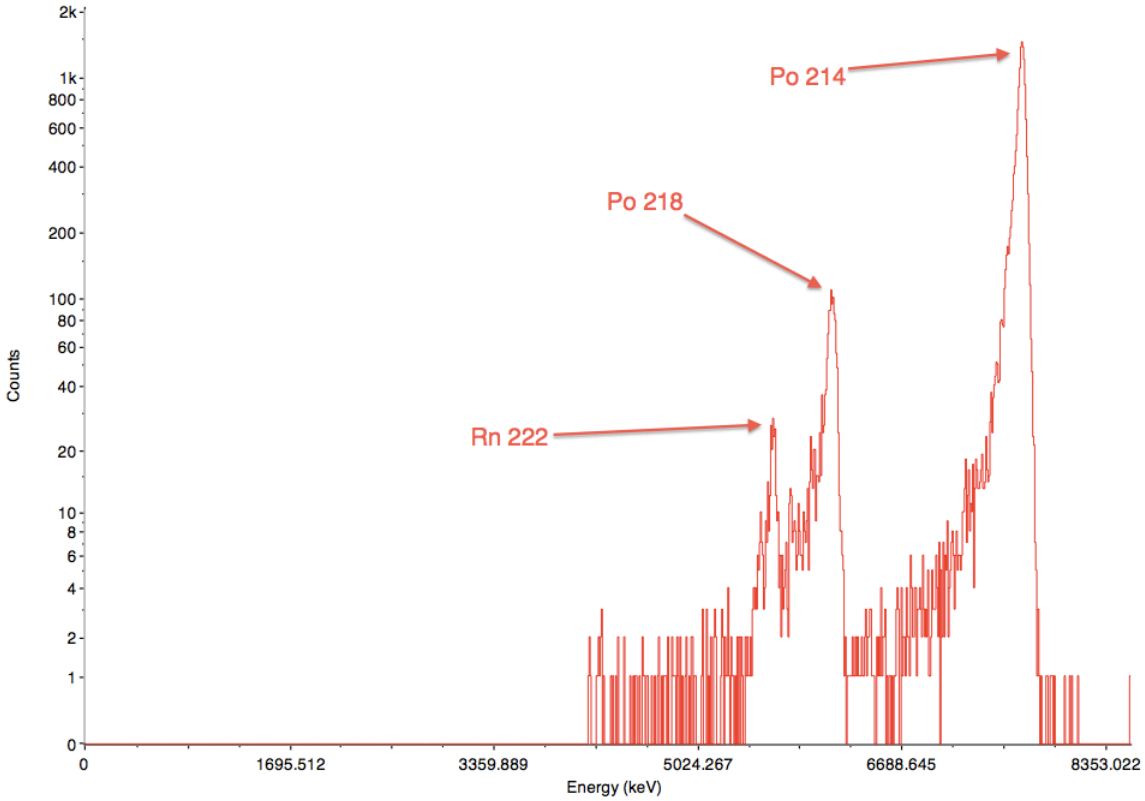

Figure 12: Calibrated spectrum of the background in the chamber immediately after source removal. The visible peaks in the ^{226}Ra decay chain have been labeled.

In doing the sort of low-background measurements of CUORE, it is important to quantify the background in the detector. To this regard, a 1200 s background spectrum was taken after removal of the source, seen in figure 12. Three very clear and distinct peaks with energies at the locations of the ^{222}Rn, ^{218}Po, and ^{214}Po were seen despite the lack of source in the chamber. The ^{226}Ra source was handled delicately in order to prevent this type of contamination.

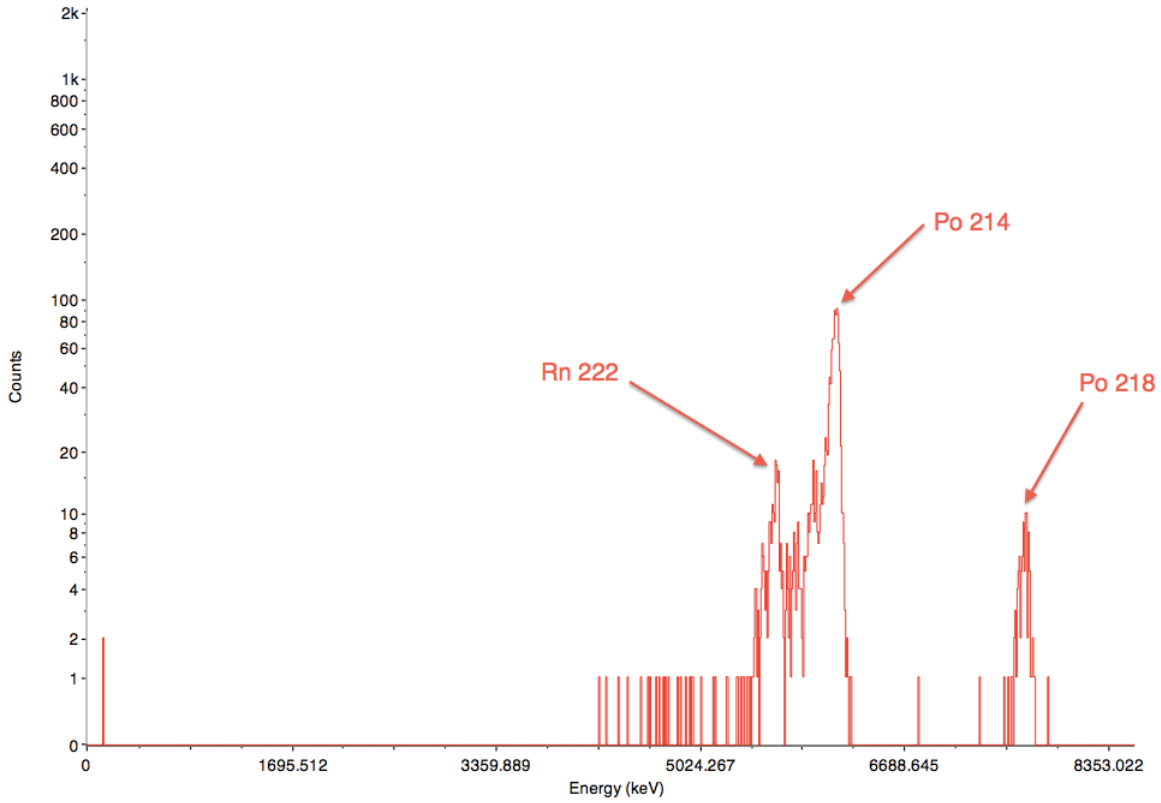

Figure 13: Calibrated spectrum of the background several hours after removal of the the ^{226}Ra source. The visible peaks in the ^{226}Ra decay chain have been labeled.

Figure 13 shows the same 1200 s background run several hours after removal of the source. The background spectrum had decayed but was still quite visible. This led to the conclusion that the chamber had been contaminated with ^{226}Ra daughters which were subsequently decaying away, which would be expected given their short half-lives. The source of this contamination was initially a mystery; however, consulting a Canberra Industries technical document revealed that the issue was likely recoil contamination [21]. In essence, recoil contamination is when an ejected alpha particle imparts enough energy on its parent nucleus to break the chemical bonds holding it in place and release it into free space. Since the chamber is held at low vacuum, it travels until it collides with another material and embeds itself slightly below the surface. Since the parent is also radioactive, it eventually will decay and emit an alpha particle. Due to the electric field in the detector, these positively charged parent nuclei are drawn to the detector and imbed themselves several microns in the silicon. This process creates a background spectrum consistent with that seen in Figure 12. This type of background is nearly impossible to remove while keeping the detector intact and steps must be taken to mitigate it [22]. As described in [22], careful control of pressure and negatively biasing the source plate in the chamber can reduce the recoil contamination by a factor of 1000.

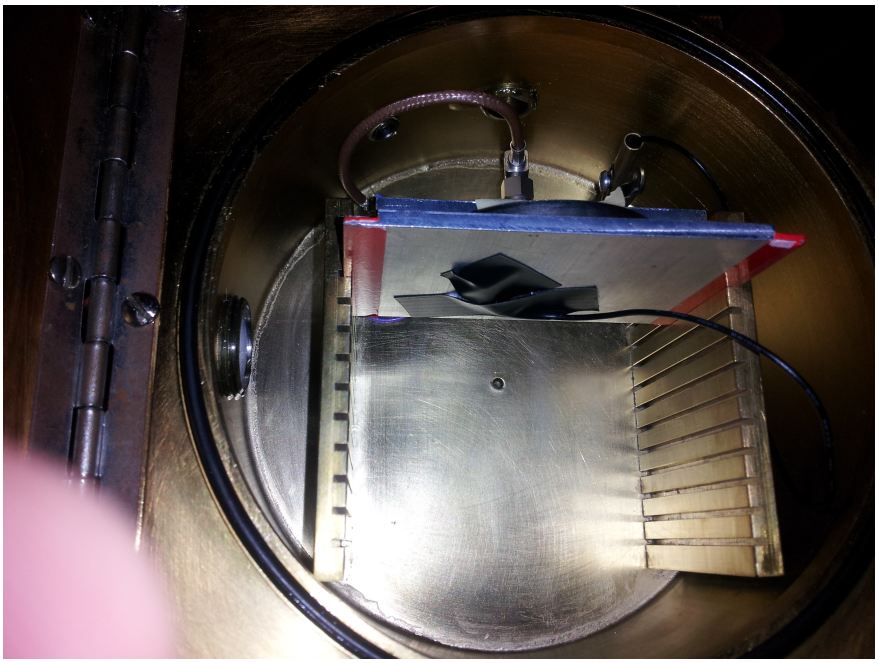

Figure 14: Negative bias is supplied to the source plate.

A -12 V power supply was fed into the chamber through a BNC feedthrough and then connected to the source plate by way of an alligator clip and electrical tape. Figure 14 shows the underside of the source plate with the negative bias attached. This method was successful in holding the source plate at -12 V while the chamber proper remained at ground. Since pressure control was not implemented at the time due to the lack of a suitable pump, the decision was made to attempt to use other calibration sources rather than ^{226}Ra in order to keep the detector uncontaminated. If samples with high activity in the common recoil contaminant chains were to be counted in the future, the pressure control system would likely have to be implemented.

By this point, it was clear the detector in use was not adequate for counting in low background applications. Prior to its use in this spectrometer, it had been used around other radioactive sources and was far too contaminated to be used for low background counting. In addition, the resolution being attained was significantly worse than the 22 keV that a new ORTEC silicon detector is rated to achieve. Two 150mm^2 detectors were located and tested in the spectrometer. Both detectors appeared to work, although one was contaminated. Slowly raising the bias voltage on both detectors while looking at the average height of the noise, it was seen that the noise decreased steadily to around 5 mV when a 100 V bias was applied and thus the decision was made to bias the 150 mm ^{2} detectors at 100 V. Due to the unavailability of a calibration pulser or another suitable calibration source, a calibration was done using both detectors, a degraded ^{252}Cf source with an unidentifiable spectrum, and a ^{226}Ra source.

Since one of the 150 mm^2 detectors was already contaminated from a previous experiment, exposing it to the ^{226}Ra source for several minutes would not contribute significantly to the overall detector contamination.

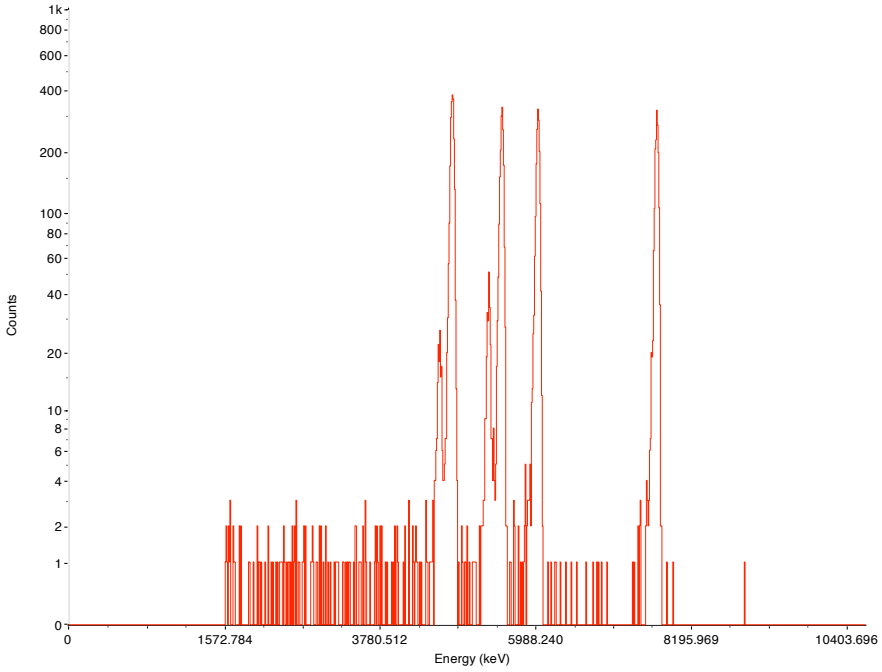

Figure 15: Spectrum for the ^{226}Ra calibration source using a 150 mm^2 ORTEC A-series detector.

This detector was calibrated using the ^{226}Ra source with the contaminated detector. The 120 second calibration run is shown in Figure 15. FWHM was found to be about 55 keV. The increase in resolution is obvious over Figure 10. A spectrum was then taken with the ^{252}Cf source with both the detectors and a shift of roughly four channels was seen with every peak in the 4500-5500 keV region. By applying a shift of four channels, a calibration for the uncontaminated detector was obtained without introducing it to the ^{226}Ra source and thus minimizing recoil contamination risk.

With this calibration, the spectrometer was in usable condition. Several improvements could have been been made and could be made in the future, primarily a cleaning of the chamber and an installation of a new silicon detector. Using the final calibration, the detector was used to try to measure the alpha radioactivity of gold (see Section 4).

3.6 Detector Geometrical Efficiency

A consideration that must be made when performing alpha spectroscopy measurements is the efficiency of detection. Since alphas lose energy rapidly in silicon, the detector itself is nearly 100% efficient. However, as alpha decay is an isotropic process, only a percentage of the alpha particles emitted from a radioactive source will reach a silicon detector some distance above the source. This percentage is known as the geometrical efficiency, G. When performing a counting measurement of a radioactive source, a correction must be made to the number of counts based on G. This takes the form of,

$$C_t = \frac{C_m}{G}, \tag{11}$$

where C_t is the total number of radioactive decays and C_m is the number of decays measured by the detector. A detector in which G=1 is known as a 4π detector and no correction is needed in such a case. Monte Carlo simulations can determine G for any geometrical arrangement given sufficient sophistication; however, this can be a tedious and involved process. Conway [23] presents the following expression for G, assuming a circular source and circular detector, as a function of R_d, the detector radius; R_s, the source radius, and h, is the height from the detector to the source, and a is the offset of the centers of the source and detector,

$$G = \frac{R_d}{R_s} \int_0^\infty \frac{J_0(as)J_1(R_d s)J_1(R_s s)}{s} exp(-sh)\,\mathrm{d}s \tag{12}$$

Conway assumes the source is two dimensional and that no alphas are absorbed by the source before entering free space. Equation 12 cannot be integrated analytically so a brief function in Mathematica was written to numerically integrate and find the geometrical efficiencies of various source detector configurations. Since silicon detectors are measured by their area and not their radius, A_d is defined as the area of the detector.

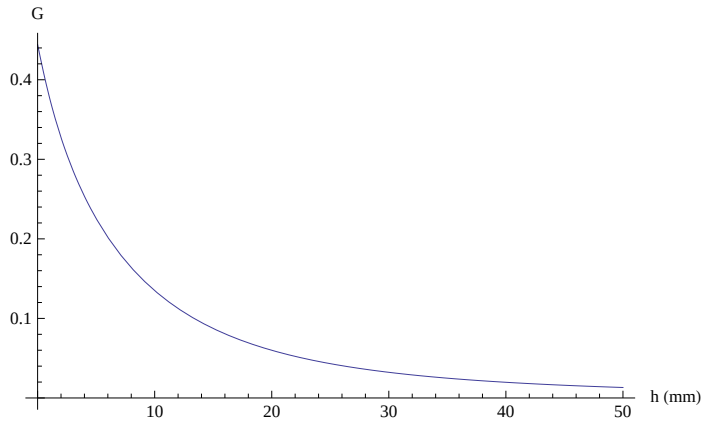

Figure 16: G as a function of h with R_s=12.7 mm and A_d=450 mm^2.

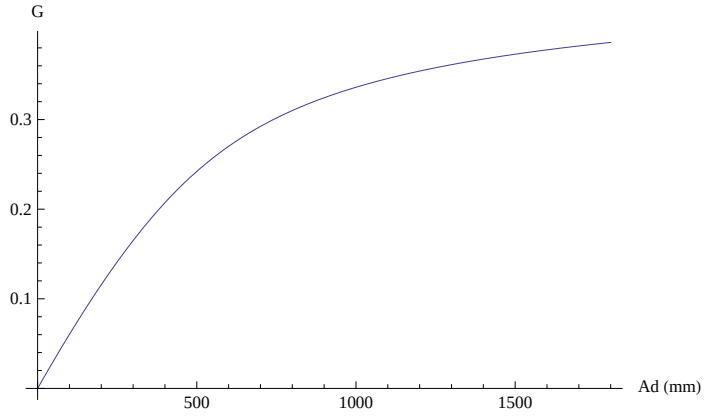

Figure 17: G as a function of A_d with R_s=12.7 mm and h=5 mm.

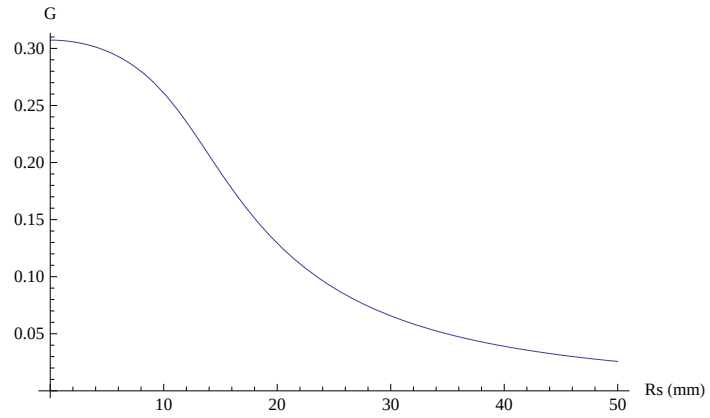

Figure 18: G as a function of R_s with A_d=450 mm^2 and h=5 mm.

Figure 16 shows that before modifications to the source or detector are made, decreasing source to detector distance offers an immediate a rapid increase in detector efficiency.

3.7 Recoil Contamination

In calibrating the alpha spectrometer, a type of contamination known as recoil contamination was seen, visible in Figure 12. This section will examine the cause and possible prevention measures for this type of introduced background. An alpha particle is emitted with a defined kinetic energy dependent on its parent nucleus. Several examples of alpha decay kinetic energies in the problematic ^{238}U decay chain are given in Table 4. Since the parent nucleus is initially at rest, conservation of momentum between the alpha daughter and the alpha particle can be used to find the energy deposited in the recoil nucleus. Solving for the γ factor of an α particle with rest mass of about 4 GeV and kinetic energy of 5 MeV using the relativistic kinetic energy formula,

$$\frac{KE_\alpha}{m_0c^2} + 1 = \gamma \tag{13}$$

we find that $\gamma = \frac{5\text{MeV}}{4\text{Gev}} + 1 \approx \frac{1}{1000} + 1 \approx 1$. This means that a natural alpha particle may be treated as non-relativistic and the following derivation of the recoil energy of the nucleus is valid. Starting with conservation of momentum,

$$m_\alpha v_\alpha = -m_d v_d, \tag{14}$$

where $m_\alpha v_\alpha$ is the momentum of the alpha particle and $m_d v_d$ is the momentum of the parent nucleus, v_d^2 can be solved for,

$$v_d^2 = \frac{m_\alpha^2}{m_d^2} V_\alpha^2. \tag{15}$$

Multiplying both sides by $\frac{1}{2}m_d$,

$$\frac{1}{2}m_d {v_d}^2 = \frac{1}{2}m_\alpha {v_\alpha}^2 (\frac{m_\alpha}{m_d}) \tag{16}$$

and knowing the non-relativistic kinetic energy is $\frac{1}{2}mv^2$, the kinetic energy of the daughter may be solved for,

$$KE_d = KE_\alpha(\frac{m_\alpha}{m_d}). \tag{17}$$

Since the mass of the alpha particle is simply the mass of a helium nucleus, the mass of the daughter is known, and the kinetic energy of the alpha particle is known, the kinetic energy imparted to the daughter nucleus, which is now traveling in a direction opposite to the incident alpha, can be found. When ^{226}Ra decays into ^{222}Rn, atomic mass of 222, it emits an alpha particle, atomic mass$\approx$4 amu, with kinetic energy 4784 keV. Simple arithmetic reveals that the ^{222}Rn nucleus is imparted with kinetic energy of 86.2 keV. This energy, much less than the energy of the emitted alpha, is enough to break the chemical bonds [21] that hold the daughter particle in place. Due to the isotropy of alpha emission, as many daughter nuclei will be emitted in the direction of the silicon detector as primary alpha particles. As the chamber is under vacuum, these daughters will travel until reaching the detector and implant themselves in the silicon. Radioactive daughters will then decay and produce a defined background. This background is what is known as recoil contamination [21]. In the worst case, the daughter of the second decay will also be radioactive and will contribute to the background as well. Since the daughters are embedded in the silicon, there is no way to remove them without destroying the detector. Not all radioactive daughters are a major source of contamination. The most troublesome contaminants are those with half-lives in the range of days or weeks. Those with short half-lives decay away rapidly and those with long half-lives do not generate a problematic level of counts [22]. Looking at the half-lives given in Table 4, it is obvious why recoil nuclei from ^{226}Ra are problematic. The initial ^{222}Rn nuclei will continue to contribute appreciable levels of background for several months. This is compounded by the fact that each of its daughters, ^{218}Po, ^{214}Po, and ^{210}Po will also decay and generate background contamination. The peaks from these decays are clearly visible in Figures 12 and 13. When trying to do ultra-low background measurements, such as vetting materials for an experiment like CUORE, even several counts per hour is an unacceptable level of contamination.

There are several ways to prevent this type of contamination. The first and most obvious is to not expose the chamber to samples with high radioactivity, especially with daughters that have half-lives on the order of a few days. If many samples all with moderate activity are counted however, recoil contamination can still build up on the detector rendering it useless for low background counting. Sill and Olsen [22] present a novel way of preventing recoil buildup. Since the recoiling daughter particles are much heavier and much less energetic than alphas, they will stop significantly more quickly when passing through an absorber than an alpha particle. Sill and Olsen found that raising air pressure to achieve a thickness of of 12 μg/cm^2 while biasing the source plate to -6 V was able to reduce recoil contamination by a factor of 1000. The negative bias must be applied in order to collect the positively charged daughter nuclei once they are stopped by the air.

4 Counting Gold

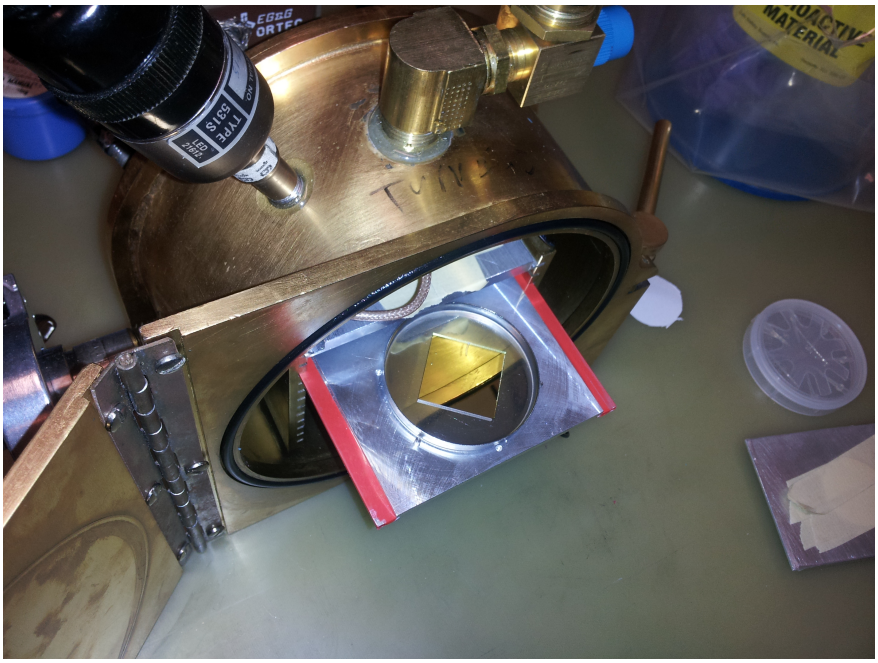

Figure 19: Vacuum chamber with gold coated glass substrate on the source tray.

With the spectrometer is working condition, a brief experiment was run to try to measure the overall radioactivity of gold. Gold is thought to have some unknown radioactive contamination and had been suggested as a bonding pad for wires in the CUORE experiment. Measuring this contamination or setting a limit on the amount of contamination present in it is important in determining whether gold is suitable for use in these bonding pads. The following section will detail this experiment and the analysis of the data.

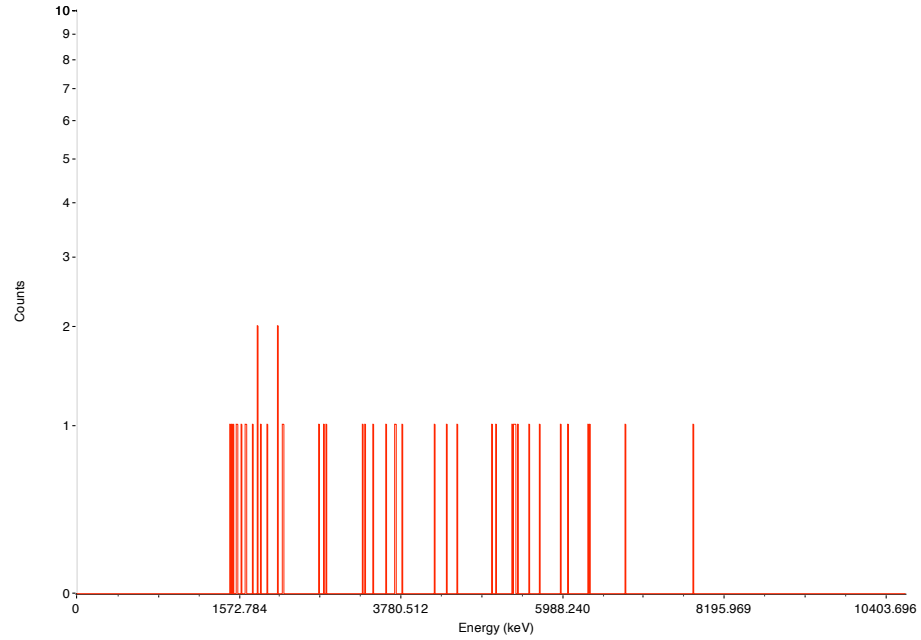

Figure 20: 90 hour count of a square inch glass substrate.

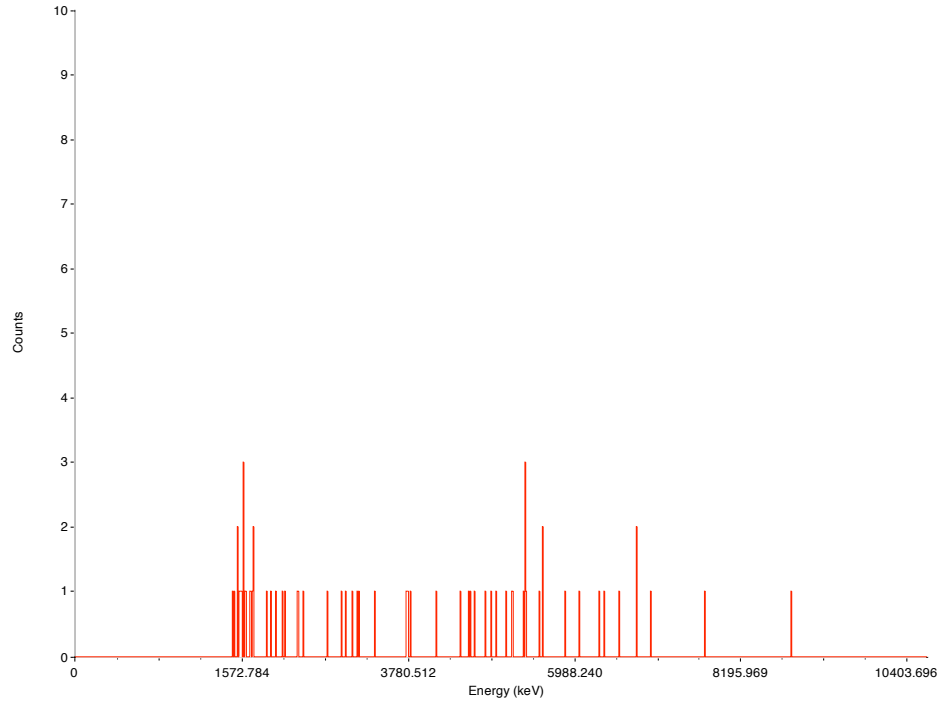

Figure 21: 120 hour count of 5000 Å thick layer of gold deposited on a square inch glass substrate.

Two 1-inch by 1-inch glass substrates were cut and cleaned using a chemical etching pro-

cess. In order to give a measure of the background, one of the substrates was counted for 90 hours and 45 counts were seen in the energy range from 2000 to 9000 keV giving a rate of $1.39\times10^{-4} \pm 2.07\times10^{-5}$ Bq, Figure 20. The other substrate had 6.485 mg of gold, roughly 5000 Å, vacuum deposited onto its surface, Figure 19. The thickness was chosen to be significantly less than the stopping distance of an alpha particle in gold. The gold was then counted for 120 hours and 66 decays were seen for a rate of $1.53\times10^{-4} \pm 1.88\times10^{-5}$ Bq (Figure 21). A value of 170.6 Bq/kg for the upper limit on the radioactivity of gold was obtained using the following toy method. The assumption was made above that the counting error in each measurement was $\sqrt{\mathrm{N}}$ where N is the number of counts. This counting error is only valid given a Poisson distribution, which is not the case for counts randomly distributed over an entire energy spectrum through multiple decay processes [24]. Still, the toy method described demonstrates that the background was too high to see any radioactivity in gold.

Assuming that the total rate of radioactive decay R_t observed by the detector is the background rate, R_b, plus R_s, the source rate, then,

$$R_s = R_t - R_b, \tag{18}$$

with error given by:

$$\delta R_s = \sqrt{\delta {R_t}^2 + \delta {R_b}^2}. \tag{19}$$

With the values given above for R_t and R_s, we see that:

$$R_s = 1.39 \times 10^{-5} \pm 2.80 \times 10^{-5} Bq. \tag{20}$$

This value is only the counts seen by the detector, not the total alpha activity of gold. A geometrical correction using Eq. 12 must be made for the true rate of decay. Eq. 12 is limited to finding the geometrical efficiency for a circular source only. To get a more accurate geometrical efficiency for the square source used, the geometrical efficiencies for a circle inscribed in a 1-inch by 1-inch square and a circle with a 1-inch by 1-inch square inscribed inside of it were averaged giving a rough geometrical efficiency of 3.7% for the 1-inch by 1-inch square glass substrate. Applying this correction yields a new value of:

$$CR_s = 3.68 \times 10^{-4} \pm 7.42 \times 10^{-4} Bq \tag{21}$$

Finally, this value can be converted to Bq per kg Au to give the value of:

$$\text{Rate} = 56.6 \pm 114 \frac{Bq}{kg} \tag{22}$$

Obviously, the error in this rate is much too high to draw any conclusions about the radioactive of gold other than setting an upper limit based on the rate plus the error. Much longer counting times, a larger detector, and cleaning the chamber to remove any alpha contamination would do yield a better value for the radioactivity of gold. This small experiment was a microcosm of the full CUORE experiment. In essence, there is a very rare decay that is buried under some amount of background contamination. In the case of the gold, the decay would be due to contaminants in very pure gold. In CUORE, it is $0\nu\beta\beta$.

5 Concluding Remarks

The discovery that neutrinos oscillate caused an uproar among the particle physics community as massive neutrinos do not fit within the current Standard Model. When CUORE begins to take data in 2015, it will attempt to probe how neutrinos fit within the Standard Model. Finding $0\nu\beta\beta$ would demonstrate both that uncharged massive particles may be their own antiparticles and that lepton number conservation can be violated. Both of these results would have implications on the current Standard Model and on theories beyond the Standard Model that predict supersymmetric analogues to known particles. A null result would further constrain the effective mass of the neutrino and thus the decay rate of $0\nu\beta\beta$. This would inform the background rates that future experiments must achieve [9]. CUORE is a synthesis of many smaller projects, such as the refurbishment of the alpha spectrometer described in this paper, all working towards the singular goal of finding $0\nu\beta\beta$.

6 References

[1] Alice Calaprice. *The New Quotable Einstein.* Princeton University Press and Hebrew University of Jerusalem, 2005.

[2] J.L. Rosner. The standard model in 2001. *arXiv preprint hep-ph/0108195*, 2001.

[3] P. Bhat. Observation of a higgs-like boson in cms at the lhc. Technical report, 2012.

[4] K Nakamura. Review of particle physics. *Journal of Physics G: Nuclear and Particle Physics*, 37(7A):075021, 2010.

[5] Dave Fehling. The standard model of particle physics: A lunchbox's guide.

[6] Brookhaven National Laboratory National Nuclear Data Center. Nudat (nuclear structure and decay data), March 18, 2008 2008.

[7] G. Choppin, JAN RYDBERG, and J.O. Liljenzin. *Radiochemistry and Nuclear Chemistry.* Chemical, Petrochemical & Process. Elsevier Science, 2001.

[8] J. J. Gomez-Cadenas, J. Martin-Albo, M. Mezzetto, F. Monrabal, and M. Sorel. The search for neutrinoless double beta decay. *Riv. Nuovo Cim.*, 35:29–98, 2012.

[9] W. Rodejohann. Neutrino-less double beta decay and particle physics. *International Journal of Modern Physics E*, 20(09):1833–1930, 2011.

[10] `http://www.lngs.infn.it/lngs_infn/index.htm?mainRecord=http://www.lngs.infn.it/lngs_infn/contents/lngs_en/research/experiments_scientific_info/experiments/current/cuore/`.

[11] F.T. Avignone III, S.R. Elliott, and J. Engel. Double beta decay, majorana neutrinos, and neutrino mass. *Reviews of Modern Physics*, 80(2):481, 2008.

[12] I. Shlimak, AN Ionov, R. Rentzsch, and JM Lazebnik. On the doping of isotopically controlled germanium by nuclear transmutation with a high concentration of shallow donor impurities. *Semiconductor science and technology*, 11(12):1826, 1999.

[13] A.D. Bryant. A search for neutrinoless double beta decay of tellurium-130. 2010.

[14] E. Andreotti, C. Arnaboldi, FT Avignone, M. Balata, I. Bandac, M. Barucci, JW Beeman, F. Bellini, C. Brofferio, A. Bryant, et al. Te130 neutrinoless double-beta decay with cuoricino. *Astroparticle physics*, 34(11):822–831, 2011.

[15] F. Alessandria, E. Andreotti, R. Ardito, C. Arnaboldi, FT Avignone III, M. Balata, I. Bandac, TI Banks, G. Bari, J. Beeman, et al. Sensitivity of cuore to neutrinoless double-beta decay. *arXiv preprint arXiv:1109.0494*, 2011.

[16] I.C. Bandac. Search for neutrinoless double beta decay with the cuore detector. *Journal of Physics: Conference Series*, 110(8):082001, 2008.

[17] F. Alessandria, R. Ardito, D. R. Artusa, and et al. Validation of techniques to mitigate copper surface contamination in cuore. *arXiv:1210.1107*, 10 2012.

[18] G.F. Knoll. *Radiation detection and measurement*. Wiley, 2010.

[19] G. Bertolini and A. Coche. Semiconductor detectors. 1968.

[20] ORTEC. An34: Experiments in nuclear science. Technical report, AMETEK, Inc.

[21] Canberra. Considerations for choosing an alpha spectroscopy pips detector. Technical report, Areve.

[22] C.W. Sill and D.G. Olson. Sources and prevention of recoil contamination of solid-state alpha detectors. *Analytical Chemistry*, 42(13):1596–1607, 1970.

[23] John T. Conway. Generalizations of ruby's formula for the geometric efficiency of a parallel-disk source and detector system. *Nuclear Instruments and Methods in Physics Research Section A: Accelerators, Spectrometers, Detectors and Associated Equipment*, 562(1):146 – 153, 2006.

[24] J.R. Taylor. *An Introduction Error Analysis: The Study of Uncertainties in Physical Measurements*. Physics - chemistry - engineering. Univ Science Books, 1997.

Resources

In addition to the articles, books, and websites listed above. Technical manuals from ORTEC and Canberra were used extensively in creating the spectrometry system and in writing this paper. Wolfram Mathematica was used for the geometric efficiency plots and general calculations used in the paper. The open source ORCA data acquisition software used for acquiring data from the 3001 and for creating the spectra presented may be found at `http://orca.physics.unc.edu/~markhowe/Orca_Help/Home.html`.

7 Glossary

Acronym	Meaning
$0\nu\beta\beta$	Neutrinoless Double Beta Decay
$2\nu\beta\beta$	Two Neutrino Double Beta Decay
CUORE	Cryogenic Underground Observatory for Rare Events
NIM	Nuclear Instrumentation Module
CAMAC	Computer Automated Measurement and Control
NTD	Neutron Transmutation Doped
FWHM	Full-Width Half-Maxiumum
SCA	Single-Channel Analyzer
MCA	Multi-Channel Analyzer
Bq	Becquerel (counts/s)

Table 5: Acronyms used in this paper, for easy reference.

8 Acknowledgments

I dedicate this paper to my parents, Jack and Gina for being the greatest parents I could ever ask for.

First and foremost, I thank my advisor, Dr. Thomas Gutierrez, for giving me the opportunity to participate in the CUORE experiment and for his guidance in this project. I would additionally like to thank my other professors, Dr. Bob Echols especially, who have instructed me in Physics while at Cal Poly. I would not be where I am today without them having pushed me to work harder and reach my fullest potential. I would also like to thank the members of the CUORE collaboration at both Gran Sasso National Laboratory and at Lawrence Berkeley National Laboratory for allowing me to take part in their research and offering counsel when needed. I would like the staff and scientists at the 88-inch Cyclotron at LBNL for offering instruction and help in acquiring materials for the project despite me being a lowly undergraduate.

Finally, I would like acknowledge the generosity and support of the late Dr. Stuart Freedman at the University of California, Berkeley. Who, with his light prodding and pushing, made this alpha spectroscopy project come to fruition.